



# Single-channel source separation and parameters estimation of multi-component BPSK/QPSK signal based on 3-D EVR spectrum and wavelet analysis

Hang Zhu<sup>1</sup> · Jian-jun Shen<sup>1</sup> · Zheng Dai<sup>1</sup> · Wei Song<sup>1</sup> · Zhong-xiang Chang<sup>1</sup>

Received: 2 February 2019 / Revised: 21 April 2019 / Accepted: 19 May 2019 / Published online: 8 June 2019  
© Springer-Verlag London Ltd., part of Springer Nature 2019

## Abstract

This paper proposes an approach of single-channel source separation and parameter estimation of multi-component rectangular pulse-shaped BPSK/QPSK (binary/quadrature phase-shift keying) signal. By structuring multi-dimensional matrix from the observed signal, we may then apply 3-D EVR spectrum to determine the delay time and symbol period and therefore to estimate the basic waveform. A cost function is designed to estimate the carrier frequency and initial phase, and the periodic ambiguity problem is solved through wavelet analysis to get accurate symbol period. Finally, the component signal can be reconstructed with estimated parameters, and the separation stops adaptively by the SNR value which is estimated with the method of subspace-based decomposition. Simulation results confirmed the effectiveness of the proposed method.

**Keywords** Multi-component signal · Symbol period · Source separation · Parameters estimation · 3-D EVR spectrum · Wavelet analysis · BPSK/QPSK signal

## 1 Introduction

As a typical digital modulation signal, the MPSK (multiple phase-shift keying) signal has the advantages of wide band of frequencies, low peak power, and good concealment and it has been used widely in radar and communication systems. For such systems, the extraction of characteristic parameters is a significant problem, and many solutions have been proposed.

At present, there are several methods used to estimate MPSK signal parameters, such as time-domain phase difference method [1, 2], wavelets [3, 4], short-time Fourier transform [5], and cyclic spectrum method [6–8]. When there is only one receiving channel in battlefield environments, it is easy to receive multiple signals at the same time; this makes it difficult to analyze multi-component mixed MPSK signals when using the above methods. Although the cyclic spectrum [9] solves the symbol rates estimation problem of two-component signals mixed in single channel, the method will be invalid when there are more than 2 components.

Single-channel source separation is a rather challenging endeavor; some researchers suggest using time–frequency distribution of sources to accomplish separation. For example, the fractional Fourier transform [10–12] is a very effective tool to process LFM signals. Li [13] used time–frequency filter and Viterbi algorithm to separate micro-Doppler signals. Liu [14] used an energy operator to estimate the modulation information of a multi-component radar signal. Adaptive decomposition [15–19] can be purposefully designed to separate multi-component frequency modulation signals. Although these methods can separate multi-component frequency modulation radar signals, they cannot be used to separate most multi-component communication signals (such as a BPSK/QPSK signal).

It is useful to accomplish separation by using the periodicity; Kanjilal [20] used singular value decomposition to successfully separate periodic source signals, Zou [21] and Cheng [22] separated periodic source signals with an algebraic approach, and Shen [23] successfully separated multi-component DSSS signal by using the periodicity of PN sequence with prior knowledge.

By analyzing the modulation period (symbol rate) of BPSK/QPSK signal, this paper is inspired to propose an effective method of source separation and parameter estimation for multi-component BPSK/QPSK signal.

✉ Hang Zhu  
taochuhang@163.com

<sup>1</sup> College of Information and Communication, National University of Defense Technology, Wuhan 430014, China

## 2 Multi-component BPSK/QPSK signal in single channel

For a single-input communication system, the received multiple-component mixed rectangular pulse-shaped BPSK/QPSK signal with noise can be written as:

$$x(t) = s(t) + v(t) = \sum_{i=1}^K s_i(t) + v(t) = \sum_{i=1}^K \{A_i \cdot U_i(t) \cdot \exp[j \cdot (2\pi f_i t + \varphi_i)]\} + v(t) \quad (1)$$

where  $v(t)$  is the complex additive white Gaussian noise with zero mean and variance  $\sigma^2$  and  $s(t)$  is the received multi-component BPSK/QPSK signal. The number of components is  $K$ . For the  $i$ th component  $s_i(t)$ ,  $A_i$  is the amplitude, where  $A_i > 0 (i = 1, 2, \dots, K)$  and  $A_1 > A_2 > \dots > A_K$ .  $f_i$  is the carrier frequency, and  $\varphi_i \in [0, \frac{\pi}{2})$  is the initial phase. The expression of the rectangular pulse sequence  $U_i(t)$  is:

$$U_i(t) = \sum_{p=1}^{\infty} b_{i,p}^{m_i} \cdot \text{rect}\left(\frac{t - (p - 1)T_{ci} - T_{ci}/2}{T_{ci}}\right) \quad (2)$$

where  $\text{rect}\left(\frac{t}{T_{ci}}\right) = \begin{cases} 1, & |t| \leq T_{ci}/2 \\ 0, & \text{otherwise} \end{cases}$ ,  $T_{ci}$  is the symbol period. The  $i$ th component is a  $m_i$ PSK signal ( $m_i = 2, 4$ );  $b_{i,p}^{m_i} = e^{j\left(\frac{q_{i,p}}{m_i} \cdot 2\pi\right)}$ , ( $q_{i,p} = 0 \sim m_i - 1$ ) is the  $p$ th symbol.

Considering the time delay  $\Gamma_i$  of each component:

$$x(t) = s(t) + v(t) = \sum_{i=1}^K s_i(t - \Gamma_i) + v(t) \quad (3)$$

With sampling period  $T_s$ , the discrete form is:

$$x[n] = x(n \cdot T_s) \quad (4)$$

## 3 Principle for the source separation and parameters estimation

### 3.1 Non-standard periodicity of BPSK/QPSK signal

A component can be represented as (when  $\tau_i = 0$ ):

$$s_i[n] = A_i \cdot U_i(nT_s) \cdot \exp[j \cdot (2\pi f_i nT_s + \varphi_i)] \quad (5)$$

$$D = \begin{bmatrix} x^{(r-1)}[\tau + 1] & x^{(r-1)}[\tau + 2] & \dots & x^{(r-1)}[\tau + M] \\ x^{(r-1)}[\tau + M + 1] & x^{(r-1)}[\tau + M + 2] & \dots & x^{(r-1)}[\tau + 2M] \\ \vdots & \vdots & \ddots & \vdots \\ x^{(r-1)}[\tau + (R - 1)M + 1] & x^{(r-1)}[\tau + (R - 1)M + 2] & \dots & x^{(r-1)}[\tau + RM] \end{bmatrix} \quad (9)$$

For positive integers  $c$  and  $d$ , we have:

$$\begin{aligned} & \left. \frac{s_i[n + cN]}{s_i[n + dN]} \right|_{N=N_{ci}} \\ &= \frac{A_i \cdot U_i(nT_s + cT_{ci}) \cdot \exp[j \cdot (2\pi f_i (nT_s + cT_{ci}) + \varphi_i)]}{A_i \cdot U_i(nT_s + dT_{ci}) \cdot \exp[j \cdot (2\pi f_i (nT_s + dT_{ci}) + \varphi_i)]} \\ &= \frac{b_{i,(c+1)}^{m_i} \cdot \exp[j \cdot (2\pi f_i cT_{ci})]}{b_{i,(d+1)}^{m_i} \cdot \exp[j \cdot (2\pi f_i dT_{ci})]} \\ &= \exp\left\{j \cdot \left[2\pi \left(\frac{q_{i,c+1} - q_{i,d+1}}{m_i} + f_i T_{ci} (c - d)\right)\right]\right\}, \quad 1 \leq n \leq N_{ci} \end{aligned} \quad (6)$$

where  $N_{ci} = T_{ci}/T_s$ , and as shown in Eq. (2),  $U_i(nT_s + cT_{ci}) = b_{i,(c+1)}^{m_i} = e^{j\left(\frac{q_{i,c+1}}{m_i} \cdot 2\pi\right)}$  when  $1 \leq n \leq N_{ci}$ . We found that the waveforms of two  $N_{ci}$  periods have repeating patterns that are scaled differently by a scale complex constant factor  $\exp\left\{j \cdot \left[2\pi \left(\frac{q_{i,c+1} - q_{i,d+1}}{m_i} + f_i T_{ci} (c - d)\right)\right]\right\}$  with unit amplitude, and it suggests that the BPSK/QPSK signal is a non-standard periodic signal [24, 25]. We can define the basic waveform  $h_i[n]$  of each component that satisfied:

$$s_i[n + (d - 1)N_{ci}] = \lambda_{dN_{ci}} \cdot h_i[n], \quad 1 \leq n \leq N_{ci} \quad (7)$$

where  $\lambda_{dN_{ci}}$  is the scale factor [24, 25].

### 3.2 Estimation of symbol period

At each separation, we remove the reconstructed component signal with maximum amplitude, so before the  $r$ th ( $r = 1, 2, \dots, K$ ) separation, the remaining signal is:

$$x^{(r-1)}[n] = x[n] - \sum_{i=1}^{r-1} \hat{s}_i[n - \hat{\tau}_i] \approx \sum_{i=r}^K s_i[n - \tau_i] + v[n] \quad (8)$$

where  $\hat{s}_i[n]$  is the reconstructed component,  $\tau_i = \Gamma_i/T_s$ ,  $\hat{\tau}_i$  is the estimated value of  $\tau_i$ , and  $x[n] = x^{(0)}[n]$ . There are  $K - r + 1$  BPSK/QPSK components in the remaining signal, and their amplitudes satisfy  $A_r > A_{r+1} > \dots > A_K$ ; then, eigenvalue decomposition (EVD) [20–22] is applied to estimate the symbol period. Consider an  $R$  row  $M$  column matrix  $D$  with time delay  $\tau = \Gamma/T_s$  expressed as:

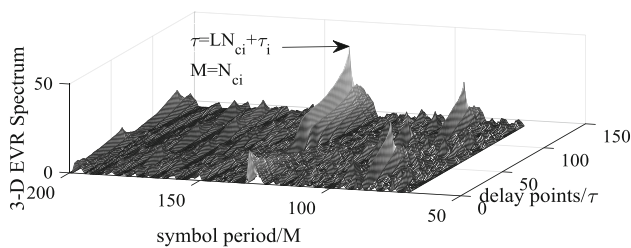


Fig. 1 3-D EVR spectrum

For different values of variables  $\tau$  and  $M$ , calculating the EVD of matrix  $D^H D$ , and we can get  $R$  eigenvalues  $\sigma_1^{(\tau, M)} > \sigma_2^{(\tau, M)} > \dots > \sigma_R^{(\tau, M)}$  and define:

$$EVR_D(\tau, M) = \frac{(R - 1)\sigma_1^{(\tau, M)}}{\sum_{i=2}^R \sigma_i^{(\tau, M)}} \tag{10}$$

Then, we get a 3-D EVR (eigenvalue ratio) spectrum EVR ( $\tau, M$ ). For  $i = r, \dots, K$ , if  $\tau - \tau_i = LN_{ci}$ , ( $L = 1, 2, \dots$ ) and  $M = N_{ci}$ , there is a peak in the 3-D spectrum corresponding to the  $i$ th components, the peak value is proportional to the amplitude  $A_i$ , and the position of the maximum peak value is  $(\tau = LN_{ci} + \tau_i, M = N_{ci})$ , as shown in Fig. 1.

Finding out the location of peak value:

$$(\tau_{\max}, M_{\max}) = \arg \max_{\tau, M} [EVR_D(\tau, M)] \tag{11}$$

where the location  $(\tau_{\max} = LN_{cr} + \tau_r, M_{\max} = \frac{N_{cr}}{P})$  is corresponding to the  $r$ th component with maximum amplitude, (the value of  $P$  will be discussed in Sect. 3.2). Here, we assume that  $M_{\max} = N_{cr}$ , then a new multi-dimensional matrix can be structured as:

$$D_{\max} = \begin{bmatrix} x^{(r-1)}[\tau_{r,m} + 1] & x^{(r-1)}[\tau_{r,m} + 2] & \dots & x^{(r-1)}[\tau_{r,m} + M_{\max}] \\ x^{(r-1)}[\tau_{r,m} + M_{\max} + 1] & x^{(r-1)}[\tau_{r,m} + M_{\max} + 2] & \dots & x^{(r-1)}[\tau_{r,m} + 2M_{\max}] \\ \vdots & \vdots & \ddots & \vdots \\ x^{(r-1)}[\tau_{r,m} + (R - 1)M_{\max} + 1] & x^{(r-1)}[\tau_{r,m} + (R - 1)M_{\max} + 2] & \dots & x^{(r-1)}[\tau_{r,m} + RM_{\max}] \end{bmatrix} \tag{12}$$

where  $\tau_{r,m} = (\tau_{\max} \bmod M_{\max})$ . Performing EVD of  $D_{\max}^H D_{\max}$  and the eigenvector corresponding to the maximum eigenvalue is the estimation  $\hat{h}_r[n]$  of  $r$ th component  $s_r[n]$ ; then, we get the carrier frequency with a rough value:

$$\tilde{f}_r = \arg \max_f \left\{ \left| \tilde{H}_r[f] \right| \right\} = \arg \max_f \left\{ \left| FFT(\hat{h}_r[n]) \right| \right\} \tag{13}$$

For  $x^{(r-1)}[n]$ , if we have estimated the time delay  $\tau_{r,m} = (\tau_{\max} \bmod M_{\max})$ , then we can get the following equation by removing the carrier frequency and initial phase (here we assumed that  $\tau_{r,m} = LN_{cr} + \tau_i, \forall i = r, \dots, K$ ):

$$\begin{aligned} x_{\Delta}^{(r-1)}[n] &= x^{(r-1)}[n + \tau_{r,m}] \cdot \text{conj}\{\exp[j \cdot (2\pi f n T_s + \varphi)]\} \\ &= \sum_{i=r}^K A_i \cdot U_i(n T_s) \cdot \exp[j \cdot (2\pi f_{\Delta i} n T_s + \varphi_{\Delta i})] \\ &\quad + v[n] \cdot \exp[-j \cdot (2\pi f n T_s + \varphi)] \\ &= \sum_{i=r}^K s_{\Delta i}[n] + v_{\Delta}[n] \end{aligned} \tag{14}$$

where  $f_{\Delta i} = f_i - \varphi$ ,  $\varphi_{\Delta i} = \varphi_i - \varphi$ , and  $U_i(n T_s) = b_{i, \lceil n/N_{ci} \rceil}^{m_i} = e^{j \left( \frac{q_i \cdot \lceil n/N_{ci} \rceil}{m_i} \cdot 2\pi \right)}$ , ( $q_i, \lceil n/N_{ci} \rceil = 0 \sim m_i - 1$ ).

Consider a cost function:

$$\begin{aligned} CF(f, \varphi) &= \frac{1}{N_{s_{\Delta r}}} \sum_n \left| \text{Re}\{x_{\Delta}^{(r-1)}[n]\} \cdot \text{Im}\{x_{\Delta}^{(r-1)}[n]\} \right|^2 \\ &= \frac{1}{N_{s_{\Delta r}}} \sum_n |CF'(f, \varphi)|^2 \end{aligned} \tag{15}$$

and let  $x_{\Delta}^{(r-1)}[n] = s_{\Delta r}[n] + w_r[n]$ , where  $w_r[n]$  is:

$$w_r[n] = x_{\Delta}^{(r-1)}[n] - s_{\Delta r}[n] = A_{w_r}[n] \cdot \exp\{j \cdot \varphi_{w_r}[n]\} \tag{16}$$

then  $CF'(f, \varphi)$  can be rewritten as:

$$\begin{aligned} CF'(f, \varphi) &= \text{Re}\{x_{\Delta}^{(r-1)}[n]\} \text{Im}\{x_{\Delta}^{(r-1)}[n]\} \\ &= \left\{ A_r \cos\left[2\pi f_{\Delta r} n T_s + \varphi_{\Delta r} + \frac{q_{\lceil n/N_{cr} \rceil}}{m_r} \cdot 2\pi\right] + A_{w_r}[n] \cdot \cos[\varphi_{w_r}[n]] \right\} \\ &\quad \cdot \left\{ A_r \sin\left[2\pi f_{\Delta r} n T_s + \varphi_{\Delta r} + \frac{q_{\lceil n/N_{cr} \rceil}}{m_r} \cdot 2\pi\right] + A_{w_r}[n] \cdot \sin[\varphi_{w_r}[n]] \right\} \end{aligned} \tag{17}$$

If  $w_r[n] = 0$ , it could be found that  $CF(f, \varphi) \geq 0$  and equality holds when:

$$\begin{aligned} 2\pi f_{\Delta r} n T_s + \varphi_{\Delta r} + \frac{q_{\lceil n/N_{cr} \rceil}}{m_r} \cdot 2\pi \\ = \frac{k\pi}{2}, \quad \forall n \in N^+, (k = 0, 1, 2, 3, \dots) \end{aligned} \tag{18}$$

where  $m_r = 2, 4$ ,  $\varphi_{\Delta r} \in (-\frac{\pi}{2}, \frac{\pi}{2})$  as  $\hat{\varphi}_r \in [0, \frac{\pi}{2})$ . In such a situation,  $\varphi_{\Delta r} = 0$  and  $f_{\Delta r} = kf_s/4$  are the necessary and sufficient condition of Eq. (18), and normally

$f_{\Delta r}/f_s \ll 1$ , so  $CF(f, \varphi)$  would be the minimum value 0 as  $(\varphi_{\Delta r} = 0, f_{\Delta r} = 0)$ .

In most cases,  $w_r[n] \neq 0$ . Since  $s_i[n]$  has the greatest amplitude among all the component signals in  $x^{(r-1)}[n]$ , there would also be a local minimum value in  $CF(f, \varphi)$  when  $\|f_{\Delta r}, \varphi_{\Delta r}\| = \|f_r - f, \varphi_r - \varphi\|$  is small enough. So we can estimate the carrier frequency and the initial phase of the  $r$ th component at the same time through a 2-D search:

$$\begin{aligned}
 (\hat{f}_r, \hat{\varphi}_r) &= \arg \min_{f, \varphi} \{CF(f, \varphi)\}, \\
 (f \in [-n_f \Delta f + \tilde{f}_r, n_f \Delta f + \tilde{f}_r], \varphi \in [0, n_\varphi \Delta \varphi], n_\varphi \Delta \varphi < \frac{\pi}{2}) & \quad (19)
 \end{aligned}$$

where  $\Delta f$  and  $\Delta \varphi$  are the search intervals and  $2n_f + 1$  and  $n_\varphi + 1$  are the numbers of search points.

### 3.3 Removal method of periodic ambiguity and optimization calculation

In Eq. (6), let  $N = \frac{N_{ci}}{P}$ , ( $P = 1, 2, 3, \dots$ ), then

$$\begin{aligned}
 & \frac{s_i[n + cN]}{s_i[n + dN]} \Big|_{N=N_{ci}/P} \\
 &= \frac{A_i \cdot U_i(nT_s + cT_{ci}/P) \cdot \exp[j \cdot (2\pi f_i(nT_s + cT_{ci}/P) + \varphi_i)]}{A_i \cdot U_i(nT_s + dT_{ci}/P) \cdot \exp[j \cdot (2\pi f_i(nT_s + dT_{ci}/P) + \varphi_i)]} \\
 &= \frac{b_{i,(\lfloor c/P \rfloor + 1)}^{m_i} \cdot \exp[j \cdot (2\pi f_i cT_{ci}/P)]}{b_{i,(\lfloor d/P \rfloor + 1)}^{m_i} \cdot \exp[j \cdot (2\pi f_i dT_{ci}/P)]} \\
 &= \exp \left\{ j \cdot \left[ 2\pi \left( \frac{q_{\lfloor c/P \rfloor + 1} - q_{\lfloor d/P \rfloor + 1}}{m_i} + \frac{f_i T_{ci}(c - d)}{P} \right) \right] \right\}, \quad 1 \leq n \leq N_{ci}/P \quad (20)
 \end{aligned}$$

which suggested that there are also several peaks in the spectrum of Eq. (10) when  $\tau + \tau_i = LN_{ci}$ , ( $L = 1, 2, \dots$ ) and  $M = N_{ci}/P$ , as shown in Fig. 2, the value of  $P$  cannot be determined directly and it can be any integer value between  $[1, \infty)$ ; we consider it be a periodic ambiguity problem and it is effective to solve the ambiguity through wavelet analysis.

Construct a single frequency signal:

$$s_{cr}[n] = \exp \left[ j \left( 2\pi \hat{f}_r n T + \hat{\varphi}_r \right) \right] \quad (21)$$

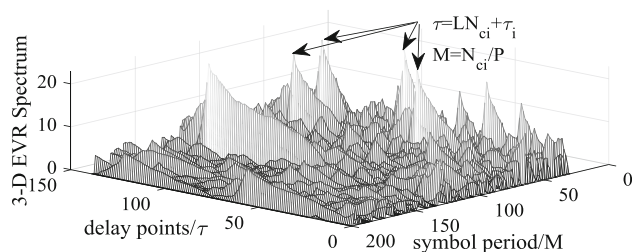


Fig. 2 Peaks with  $\tau + \tau_i = LN_{ci}$  and  $M = N_{ci}/P$

and it can be used to generate a reference signal  $s_{rr}[n]$  which can approximately fit the symbol changes  $s_r[n]$ :

$$\begin{aligned}
 s_{rr}[n + LM_{\max}] & \\
 &= \exp \left\{ j \cdot \text{phase} \left[ \frac{1}{M_{\max}} \sum_{m=1}^{M_{\max}} x^{(r-1)}[\tau_{r,m} + m + LM_{\max}] s_{cr} * [m] \right] \right\}, \\
 (n = 1, 2, \dots, M_{\max}; L = 0, 1, \dots) & \quad (22)
 \end{aligned}$$

where  $\tau_{r,m} = (\tau_{\max} \bmod M_{\max})$ .

We can get the wavelet coefficient spectrums with different scales  $a$  by making continuous Haar wavelet transform to  $\text{Re}[s_{rr}[n]]$  or  $\text{Im}[s_{rr}[n]]$ :

$$\text{RWC}_r[a, n] = \text{CWT}_{\text{Haar}}\{\text{Re}[s_{rr}[n]]\} \quad (23a)$$

$$\text{IWC}_r[a, n] = \text{CWT}_{\text{Haar}}\{\text{Im}[s_{rr}[n]]\} \quad (23b)$$

As shown in Fig. 3, the positions where symbol value changes are distinguishable in the spectrograms. We may get the average waveform to get more accurate information:

$$\text{AWC}_r[n] = \sum_a |\text{RWC}_r[a, n]| + \sum_a |\text{IWC}_r[a, n]| \quad (24)$$

The symbol period of the component  $s_r[n]$  could be estimated accurately by finding out the greatest common divisor of all the peak intervals in  $\text{AWC}_r[n]$ , as shown in Fig. 4. For  $\text{AWC}_r[n]$ , we only retain the values large enough:

$$\text{AWC}_r[n] = \begin{cases} \text{AWC}_r[n], & \text{AWC}_r[n] \geq 0.6 \max\{\text{AWC}_r[n]\} \\ 0, & \text{otherwise} \end{cases} \quad (25)$$

Then, assuming that there are  $r_p$  peaks in  $\text{AWC}_r[n]$ , let  $P_{\text{AWC}_r}[m] = \text{Findpeaks}\{\text{AWC}_r[n]\} = [n_1, n_2, \dots, n_{r_p}]$  be the vector contains all the locations of peaks, and the accurate symbol period can be estimated:

$$M_{pr} = \min_{\geq M_{\max}} \{|\text{LOC}[m]|\} \quad (26)$$

where  $\text{LOC}[m] = \text{diff}\{P_{\text{AWC}_r}[m]\} = [n_2 - n_1, n_3 - n_2, \dots, n_{r_p} - n_{r_p-1}]$  means the difference vector. With Eq. (26), we can get the minimum value among all the peak intervals which are not smaller than  $M_{\max}$  and therefore solved the problem of periodic ambiguity; if  $M_{\max}$  changed

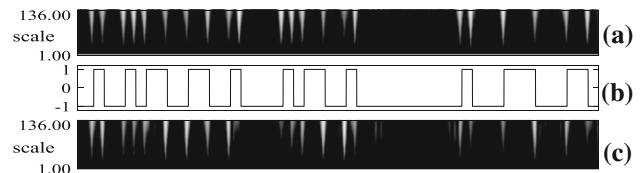


Fig. 3 Wavelet coefficient **a**  $\text{RWC}[a, n]$ , **b** symbol sequence, **c**  $\text{IWC}[a, n]$

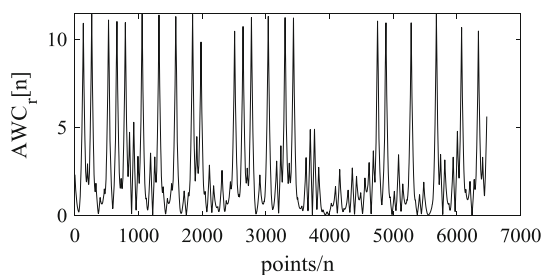


Fig. 4 The average waveform of  $AWC_r[n]$

compared with the value gotten through Eq. (11), then let  $M_{\max} = M_{pr}$  be the accurate symbol period and re-estimate the time delay  $\tau_{\max} = \arg \max_{\tau} SVR_D(\tau, M_{\max})$  and  $\tau_{r,m} = (\tau_{\max} \bmod M_{\max})$ .

In Eq. (19), we have got good estimation values of carrier frequency and initial phase; in order to improve estimation accuracy, we may apply gradient steepest descent method to do an optimization calculation to increase estimation precise. The derivative functions are given as:

$$\frac{dCF(f, \varphi)}{df} = \sum_n 2\text{Re} \left\{ -j2\pi n \cdot y[n] \left[ 2(x_{\Delta}^{(r-1)}[n])^2 + 2(x_{\Delta}^{(r-1)} * [n])^2 \right] \right\} \tag{27a}$$

$$\frac{dCF(f, \varphi)}{d\varphi} = \sum_n 2\text{Re} \left\{ -j \cdot y[n] \left[ 2(x_{\Delta}^{(r-1)}[n])^2 + 2(x_{\Delta}^{(r-1)} * [n])^2 \right] \right\} \tag{27b}$$

where  $y[n] = \text{Re}(x_{\Delta}^{(r-1)}[n]) \cdot \text{Im}(x_{\Delta}^{(r-1)}[n])$ .

### 3.4 Amplitude estimation

Get a new  $s_{cr}[n]$  in Eq. (21) with updated carrier frequency and initial phase and then get a new reference signal  $s_{sr}[n]$ :

$$s_{sr}[n + LM_{\max}] = s_{cr}[n] \cdot \exp \left\{ j \cdot \text{phase} \left[ \frac{1}{M_{\max}} \sum_{m=1}^{M_{\max}} x^{(r-1)}[\tau_{r,m} + m + LM_{\max}] s_{cr} * [m] \right] \right\}, \tag{28}$$

$(n = 1, 2, \dots, M_{\max}; L = 0, 1, \dots)$

which can be used to obtain the amplitude:

$$\hat{A}_r = \left| \frac{\sum_{n=1}^{\text{length}[s_{sr}]} x^{(r-1)}[\tau_{r,m} + n] s_{sr} * [n]}{\text{length}[s_{sr}]} \right|. \tag{29}$$

Then, the component signal can be reconstructed as:

$$\hat{s}_r[n] = \left[ [O_{1 \times \tau_{r,m}}, \hat{A}_r \cdot s_{sr}[n]] \right] \tag{30}$$

We may remove it to get  $x^{(r)}[n] = x^{(r-1)}[n] - \hat{s}_r[n]$ , and the remaining components can also be reconstructed by repeating the steps in this section with the new mixture.

### 3.5 Stopping separation adaptively by estimating SNR

In this paper, we apply the subspace-based decomposition to estimate SNR [26–28] and assume that the energy of each component is not too small compared with noise; so for the remaining signal  $x^{(r)}[n]$  after  $r$ th separation, if the estimated signal–noise ratio  $\text{SNR}_r < \text{TH}$  (TH is the threshold with small value), then, the separation should be stopped.

Here, we introduce the concept of waveform similarity as shown in Eq. (31) to measure the level of similarity of source and reconstructed signals, where  $\rho(y, s)$  is the similarity coefficient,  $y(t)$  and  $s(t)$  are the reconstructed and source signals, and  $E[\cdot]$  means the value of expectation. For 300 different sets of parameters, we used the proposed method to complete estimation of mono-component BPSK/QPSK signal under different SNRs; we find that when  $\text{SNR} < -8$  dB, the mean waveform similarity value is lower than 0.8; in this case, we consider that the reconstruction performance is not good. For the multi-component signal, in order to get a better reconstruction effect, the threshold can be set  $\text{TH} = -8$  dB as an empirical value. In Fig. 5, we give out the flowchart of the proposed method.

$$\rho(y, s) = \frac{|E[y(t)s(t)]|}{\sqrt{|E[y^2(t)]E[s^2(t)]|}} \tag{31}$$

## 4 Simulation and analysis

In simulation, we use the method to analyze a three-component BPSK/QPSK signal in single channel, the signal is under Gaussian white noise, and the SNR is 10 dB. The parameters are shown in Table 1.

The sampling frequency is 1 MHz, and we use 13,200 samples of the signal to complete the analysis.

In Fig. 6, we give the process of estimation of delay time and symbol period; here, we got that  $M_{\max} = \frac{132}{P=3} = 44$  and  $\tau_{r,m} = 10$ , and then by using EVD, we can get the basic waveform and estimate the carrier frequency with a rough value  $\tilde{f}_r = 227.7$  kHz, which is shown in Fig. 7.

The more accurately estimated value can be obtained through 2-D search with  $CF(f, \varphi)$ , as shown in Fig. 8,  $(\hat{f}_1, \hat{\varphi}_1) = (230 \text{ kHz}, 1.382)$ ; For the cost function  $CF(f, \varphi)$ , to escape from local traps; it is necessary to improve accuracy of the 2-D search by reducing search intervals  $\Delta f$  and  $\Delta \varphi$  to make the initial value of optimization calculation better; in this simulation, we set that  $(\Delta f = 50, \Delta \varphi = \pi/200)$ .



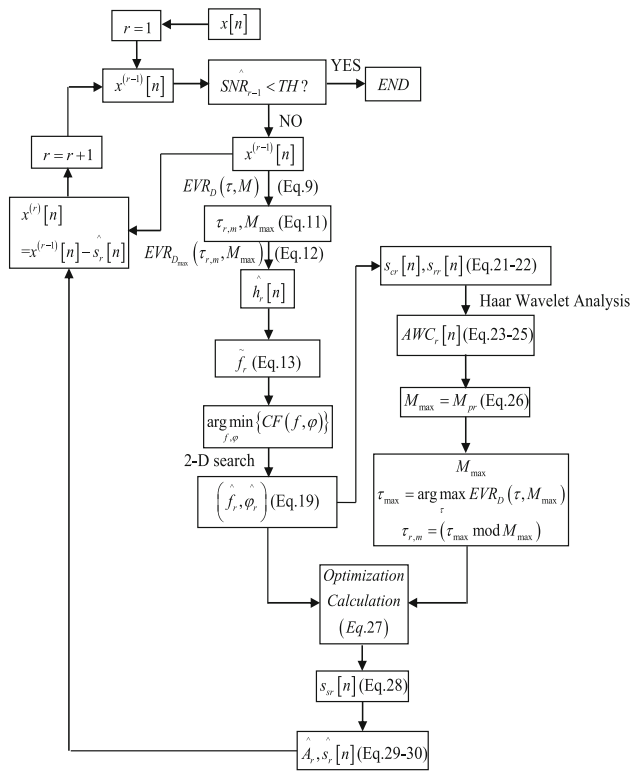


Fig. 5 The flowchart of the method proposed in this paper

The waveform of  $AWC_1[n]$  is given in Fig. 9, from which we can estimate the accurate symbol period  $N_{c1} = M_{p1} = 132$  by finding out the greatest common divisor of all the peak intervals. Let  $M_{max} = M_{p1} = 132$ , we can re-estimate the time delay  $\tau_{r,m} = 10$  through EVR spectrum with  $M=132$ , as shown in Fig. 10. After optimization calculation with gradient steepest descent method, we finally get  $(\hat{f}_1, \hat{\phi}_1) = (230.0015 \text{ kHz}, 1.2501)$ , and then we can estimate the amplitude  $\hat{A}_1 = 0.8122$ ;

The estimated values of the parameters are shown in Table 2, the constellation diagrams of all the reconstructed signals are shown in Fig. 11, and the symbol information sequences after demodulation with estimated parameters are shown in Fig. 12 compared with sources. After the third separation, the estimated  $\widehat{SNR}_3 = -10.9165 \text{ dB}$  and it is smaller than the threshold  $TH = -8 \text{ dB}$ , so the separation can stop.

In Fig. 13, we give the estimation precision (NRMSE curves) of all the parameters under different sampling fre-

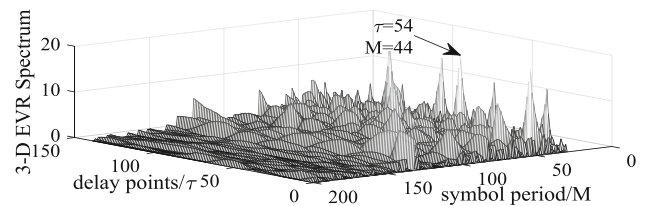


Fig. 6 The search process of 3-D EVR spectrum

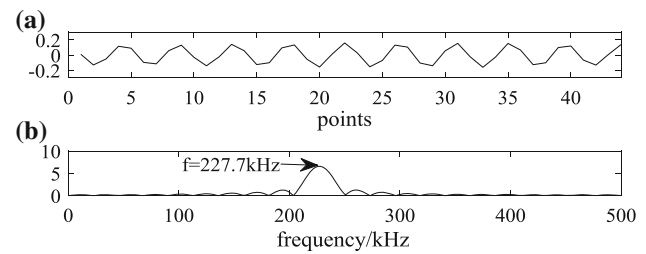


Fig. 7 The estimated basic waveform a time domain and b frequency domain

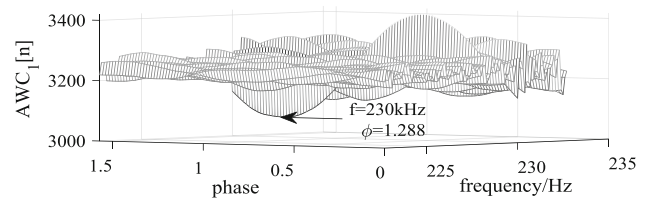


Fig. 8 2-D search for carrier frequency and initial phase

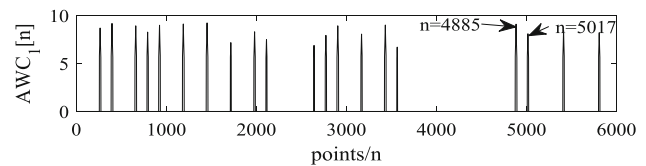


Fig. 9 The waveform of  $AWC_1[n]$

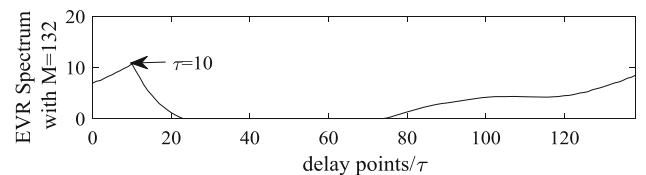


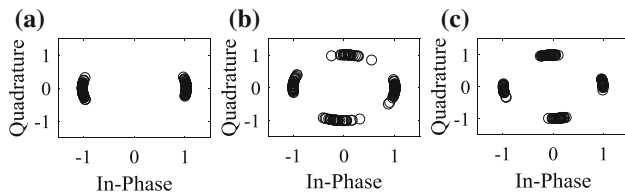
Fig. 10 Re-estimation of delay time through EVR spectrum with  $M = 132$

Table 1 All the parameters of the multi-component BPSK/QPSK signal

	$A_i$	$f_i$ (kHz)	$\phi_i$	$\tau_i$	$N_{ci}$	Modulation type
Component 1( $i = 1$ )	0.8	230.002	$2\pi/5$	10 sample points	132 sample points	BPSK
Component 2( $i = 2$ )	0.6	240.003	$\pi/4$	20 sample points	95 sample points	QPSK
Component 3( $i = 3$ )	0.3	250.004	$\pi/3$	30 sample points	114 sample points	QPSK

**Table 2** Comparison of the estimated and the true parameters

	$A_i$	$f_i$ (kHz)	$\varphi_i$	$\tau_i$ /points	$N_{ci}$ /points	Waveform similarity	Estimated SNR
Component 1 ( $i = 1$ )	0.8	230.002	$2\pi/5$	10	132	0.9883	6.4026
Reconstructed signal 1	0.8122	230.0015	1.2501	10	132		
Component 2 ( $i = 2$ )	0.6	240.003	$\pi/4$	20	95	0.9861	- 0.5491
Reconstructed signal 2	0.6153	240.0051	0.7443	20	95		
Component 3 ( $i = 3$ )	0.3	250.004	$\pi/3$	30	114	0.9908	- 10.9164
Reconstructed signal 3	0.3017	250.0023	1.0401	30	114		



**Fig. 11** The constellation diagrams of the reconstructed signals **a** component 1, **b** component 2, and **c** component 3

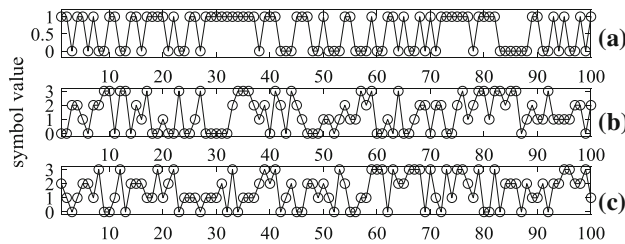


**Fig. 12** The symbol sequences after demodulation for **a** component 1, **b** component 2, and **c** component 3

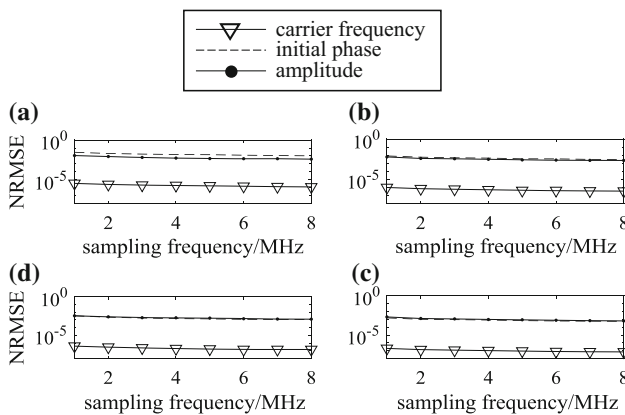


**Fig. 13** The NRMSE curves of different sampling frequencies and SNRs **a** 5 dB, **b** 10 dB, **c** 15 dB, and **d** 20 dB

quencies ( $F_s = 1-8$  MHz) and SNRs, and we see that there are more accurate results with high sampling frequency.

Some times, the value  $T_{ci}/F_s$  may not be a integer when the sampling frequency is not appropriate, so by searching the peak of EVR spectrum when changing  $M$  by step value 1, the resulting value of  $M_{max}$  is only the integer part of  $T_{ci}/F_s$ . In order to avoid this situation, we may re-search the peak

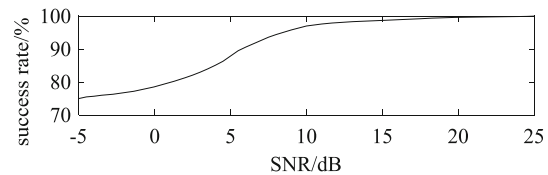


**Fig. 14** The success rate of estimation of delay times and symbol periods

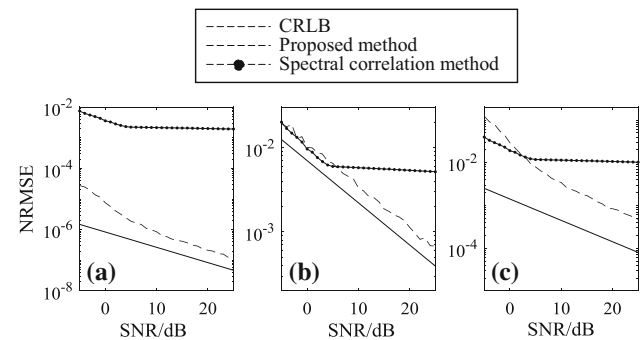


**Fig. 15** The NRMSE and the CRLB curves of parameters **a** carrier frequency, **b** initial phase, and **c** amplitude

of the spectrum of the advanced matrix shown as Eq. (32) by changing the value  $M$  with step value 0.01 within a small range around  $M_{max}$ .

By using the advanced matrix of Eq. (32) and searching the location  $\hat{M}_{max}$  of peak value,  $\hat{M}_{max}$  may be not an integer, if  $\left| \frac{\hat{M}_{max} - M_{max}}{M_{max}} \right| \leq \delta_c$  (where  $\delta_c$  is a very small value), we can consider that the sampling frequency is appropriate; otherwise, let  $F_s = F_s \cdot \left( \frac{M_{max}}{\hat{M}_{max}} \right)$  be the appropriate one to complete separation.

In Fig. 14, we give the success rate that the delay times and symbol periods of all the components were estimated correctly.

The NRMSE curves of the three parameters under different input SNRs are drawn in Fig. 15 when there is only one-component signal and the CRLB curves are also shown in this figure. In addition, we compare the estimation performance with the spectral correlation method. It can be seen from Fig. 15 that the precision of the proposed method is higher than the spectral correlation method under high SNR, and its advantage lies in its ability to deal with single-channel multi-component problems.

$$D = \begin{bmatrix} x^{(r-1)}[\tau + 1] & x^{(r-1)}[\tau + 2] & \cdots & x^{(r-1)}[\tau + \lceil M \rceil] \\ x^{(r-1)}[\tau + \lceil M \rceil + 1] & x^{(r-1)}[\tau + \lceil M \rceil + 2] & \cdots & x^{(r-1)}[\tau + 2\lceil M \rceil] \\ \vdots & \vdots & \ddots & \vdots \\ x^{(r-1)}[\tau + \lceil (R-1)M \rceil + 1] & x^{(r-1)}[\tau + \lceil (R-1)M \rceil + 2] & \cdots & x^{(r-1)}[\tau + \lceil (R-1)M \rceil + \lceil M \rceil] \end{bmatrix} \quad (32)$$

## 5 Conclusion

This paper proposes a useful method of single-channel source separation and parameters estimation of multi-component BPSK/QPSK signal. Simulation results indicate that the method is effective with a high estimation precision. Future studies would be needed to construct an advanced cost function with limitations or improve resolution method to reduce computation of 2-D search and optimization calculation. Further, it is also necessary to consider the situation that the component signal is shaped by more complex pulse shaping filter and modulated with more complex digital phase modulation system.

## References

1. Yu Z. H., Shi Y. Q., Su W.: A blind carrier frequency estimation algorithm for digitally modulated signals. In: Military Communications Conference, Monterey, USA, pp. 48–53 (2004)
2. Li, Y., Li, G.T., Yang, G.Q.: Automatic digital modulation recognition algorithm of communication signals. *J. Electron. Inf. Technol.* **27**(2), 197–201 (2005)
3. Ho, K.C., Prokopiw, W., Chan, Y.T.: Modulation identification of digital signals by the wavelet transform. *IEE Proc.—Radar Sonar Navig.* **147**(4), 169–176 (2000)
4. Wang, L., Zhang, G.X., Bian, D.M.: Blind symbol rate estimation of satellite communication signal by Haar wavelet transform. *J. Electron.* **28**(2), 198–203 (2011)
5. Djurovic, Igor: Estimation of sinusoidal frequency-modulated signal parameters in high-noise environment. *Signal Image Video Process.* **11**(8), 1537–1541 (2017)
6. Jin, Y., Ji, H.B.: A new cyclic autocorrelation based blind parameter estimation method for PSK signals. *J. Xidian Univ.* **33**(6), 892–901 (2006)
7. Wen J.Y.: Parameter estimation in detection of BPSK radar signals. In: IET International Radar Conference 2009, Guilin, China, pp. 1–4 (2009)
8. Cui, W.L., Jiang, H., Li, J.Q.: Improved fast cyclic spectral estimation algorithm and performance analysis. *J. Electron. Inf. Technol.* **33**(7), 1594–1599 (2011)
9. Yu, N.Y., Ma, H.G., Shi, R.: Blind estimation of symbol rates of multi-component phase-shift Keying signals. *J. Southwest Jiaotong Univ.* **46**(6), 904–909 (2011)
10. Hao, H.Y.: Multi-component LFM signal detection and parameter estimation-based on EEMD–FRFT. *Optik* **124**, 6093–6096 (2013)
11. Durak, L., Aldirmaz, S.: Adaptive fractional Fourier domain filtering. *Signal Process.* **90**, 1188–1196 (2010)
12. Almeida, L.B.: The fractional Fourier transform and time-frequency representations. *IEEE Trans. Signal Process.* **42**, 3084–3091 (1994)
13. Li, P., Wang, D.C., Wang, L.: Separation of micro-Doppler signals based on time frequency filter and Viterbi algorithm. *Signal Image Video Process.* **1**(7), 593–605 (2007)
14. Liu, Y.: A fast and accurate single frequency estimator synthetic approach. *Acta Electron. Sin.* **27**(6), 126–128 (1999)
15. Zou, H., Bao, Z.: An efficient algorithm for adaptive Chirplet-based decomposition. *Acta Electron. Sin.* **29**(4), 515–517 (2001)
16. Zhu, H., Zhang, S.N., Zhao, H.C.: Single-channel source separation of radar fuze mixed signal using advanced adaptive decomposition. *Acta Phys. Sin.* **63**(5), 058401 (2014)
17. Yin, Q.Y., Qian, S., Feng, A.G.: A fast refinement for adaptive Gaussian Chirplet decomposition. *IEEE Trans. Signal Process.* **50**(6), 1298–1306 (2002)
18. Hu, X.Y., Peng, S.L., Hwang, W.L.: Multicomponent AM-FM signal separation and demodulation with null space pursuit. *Signal Image Video Process.* **7**(7), 1093–1120 (2013)
19. Khan, N.A., Mohammadi, M., Ali, S.: Instantaneous frequency estimation of intersecting and close multi-component signals with varying amplitudes. *Signal Image Video Process.* **13**(3), 517–524 (2019)
20. Kanjilal, P.P.: Fetal ECG extraction from single-channel maternal ECG using singular value decomposition. *IEEE Trans. Biomed. Eng.* **44**(1), 51–59 (1997)
21. Zou M.Y., Chai Z.M., Unbehauen R.: Separation of periodic signals by using an algebraic method. In: Proceedings of the 1991 IEEE International Symposium on Circuits and Systems, Beijing, China, pp. 2427–2430 (1991)
22. Cheng H., Tang B., Du J.J.: Single channel pulse train radar signal separation using algebraic method. In: Proceedings of IEEE Radar Conference 2009, Guilin, China, pp. 382–385 (2009)
23. Shen, L., Sheng, D., Sun, M.H.: Anti-jamming algorithm of spread spectrum communication based on blind source separation in single channel. *Chin. J. Radio Sci.* **29**(5), 922–927 (2014)
24. Zhu, H., Zhang, S.N., Zhao, H.C.: Single-channel source separation of multi-component radar signal with the same generalized period using ICA. *Circuits Syst. Signal Process.* **35**, 353–363 (2015)
25. Zhu, H., Zhang, S.N., Zhao, H.C.: Single channel source separation and parameter estimation of multi-component PRBCPM-SFM signal based on generalized period. *Digit. Signal Process.* **40**, 224–237 (2015)
26. Andersin M., Mandayani N.B., Yates R.D.: Subspace based estimation of the signal to interference ratio for TDMA cellular systems. In: IEEE Vehicular Technology Conference, Atlanta, USA, pp. 1155–1159 (1996)
27. Ramakrishna, D., Mandayani, N.B., Yates, R.D.: Subspace based SIR estimation for CDMA cellular systems. *IEEE Trans. Veh. Technol.* **49**(5), 1732–1742 (2002)
28. Zhang, J.C., Peng, H.: Robust blind SNR estimation method based on subspace decomposition. *J. Data Acquis. Process.* **26**(5), 609–614 (2011)

**Publisher's Note** Springer Nature remains neutral with regard to jurisdictional claims in published maps and institutional affiliations.